Supporting information
Piezoelectric Energy Harvesting of a Bismuth Halide Perovskite Stabilised by Chiral Ammonium Cations

Supriya Sahoo, Nilotpal Deka, Ramamoorthy Boomishankar*
Department of Chemistry and Centre for Energy Science, Indian Institute of Science Education and Research (IISER), Pune, Dr. Homi Bhabha Road, Pune – 411008, India
CCDC No. 2181247 (1-S-298 K) & 2181248 (1-S-100 K)

Table of contents

Table S1. X-ray Crystallographic data for **1-S**.

Crystallographic details	**1-S**	**1-S**
Chemical formula	C_{18} H_{28} Br_5 N_2 Bi	C_{18} H_{28} Br_5 N_2 Bi
Formula weight (g/mol)	880.95	880.95
Temperature	100(2)K	298(2)K
Crystal system	Orthorhombic	Orthorhombic
Space group	P_{212121}	P_{212121}
a (Å); α (°)	7.903(2); 90	8.016(3); 90
b (Å); β (°)	14.943(4); 90	15.184(7); 90
c (Å); γ (°)	21.449(6); 90	21.635(9); 90
V (Å^3); Z	2533.0(12); 4	2633.4(19); 4
ρ (calc.) g cm^{-3}	2.310	2.222
μ(Mo K_α) mm^{-1}	14.854	14.288
$2\theta_{max}$ (°)	50.04	54.04
R(int)	0.2107	0.1010
Completeness to θ	99.8	99.7
Data / param.	4478/242	4648/241
GOF	1.102	1.123
R1 [F>4σ(F)]	0.0773	0.0448
wR2 (all data)	0.0933	0.0764
max. peak/hole (e.Å^{-3})	1.481/-1.522	1.483/-1.306

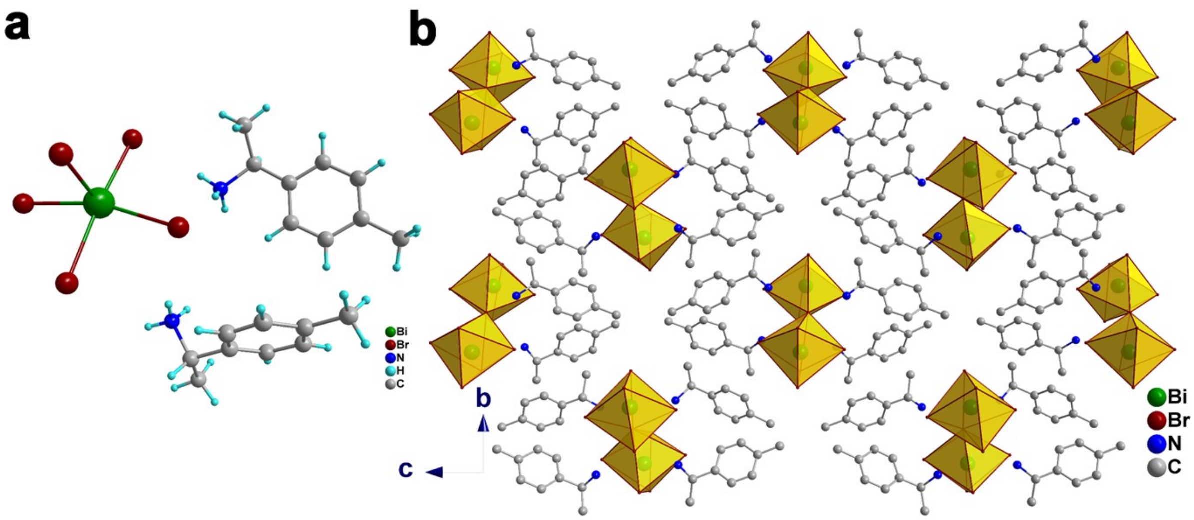

Figure S1. (a) Asymmetric unit and (b) packing diagram of **1-S** along a-axis at 100 K.

Table S2. Hydrogen bonding parameters for **1-S**.

D-H···A	d(H···A) Å	d(D-A) Å	<(DHA)	Symmetry transformations to generate equivalent atoms
N(11)-H(11D)···Br4	2.5205(25)Å	3.4234(238) Å	172.887(1492)	-0.5+x, 0.5-y, 1-z
N(11)-H(11F)···Br2	2.5862(26)Å	3.4088(214) Å	150.45(129)	0.5+x, 0.5-y, 1-z
N(21)-H(21D)···Br4	2.6226(26)Å	3.4911(255) Å	159.588(1597)	-0.5+x, 0.5-y, 1-z
N(21)-H(21F)···Br1	2.5001(32)Å	3.3726(239) Å	161.443(1499)	-0.5+x, 0.5-y, 1-z

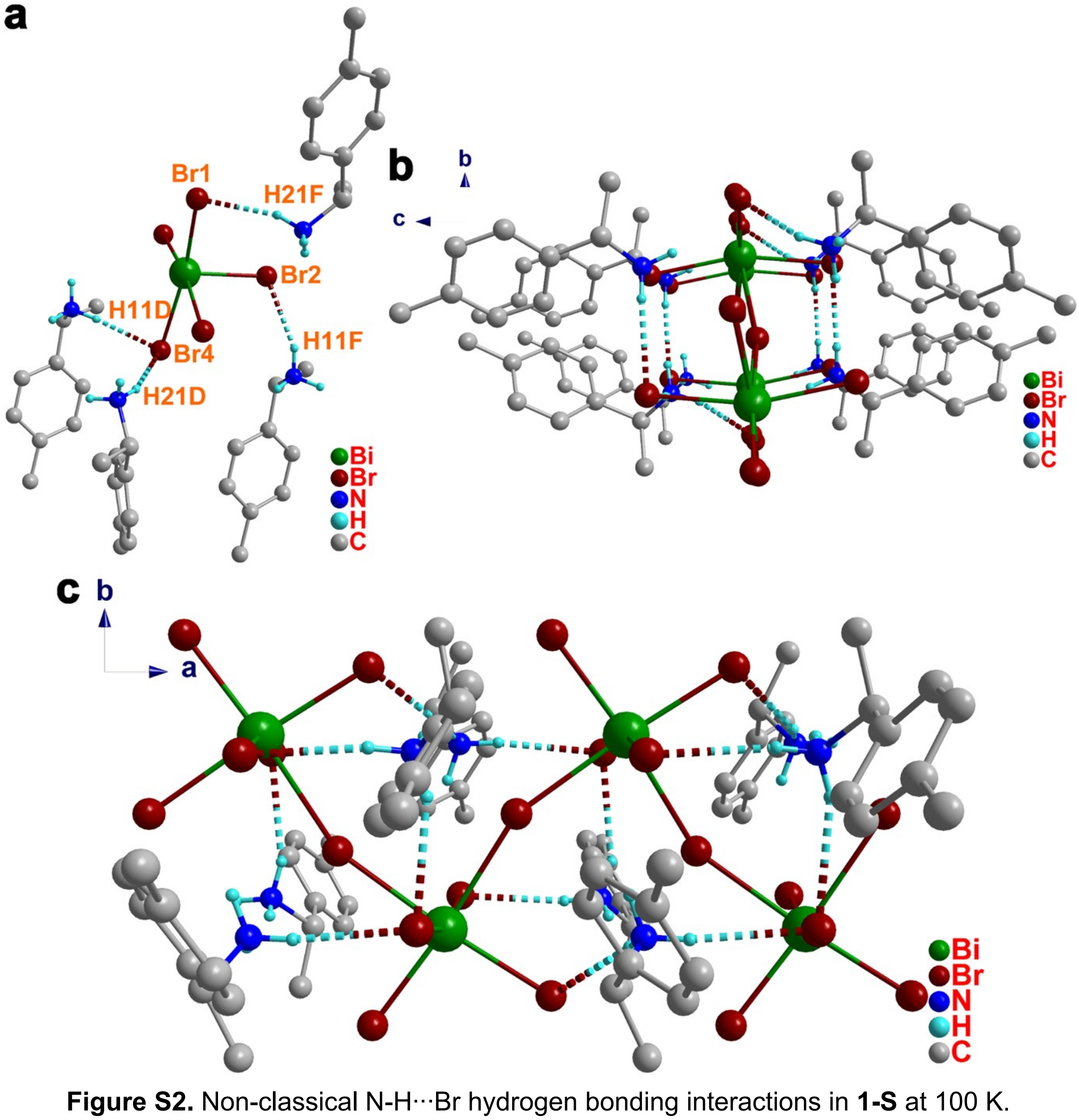

Figure S2. Non-classical N-H···Br hydrogen bonding interactions in **1-S** at 100 K.

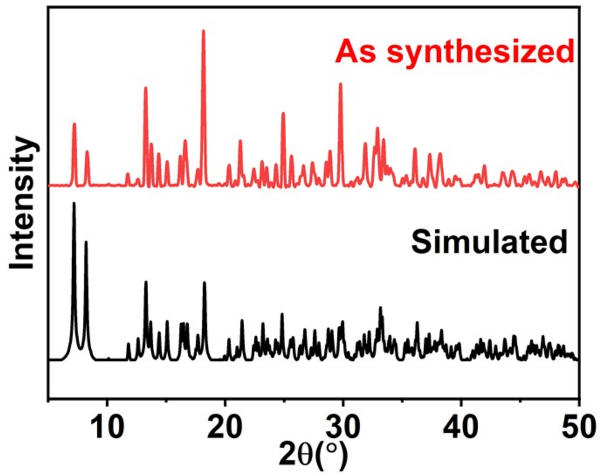

Figure S3. The powder X-ray diffraction (PXRD) profile of **1-S**.

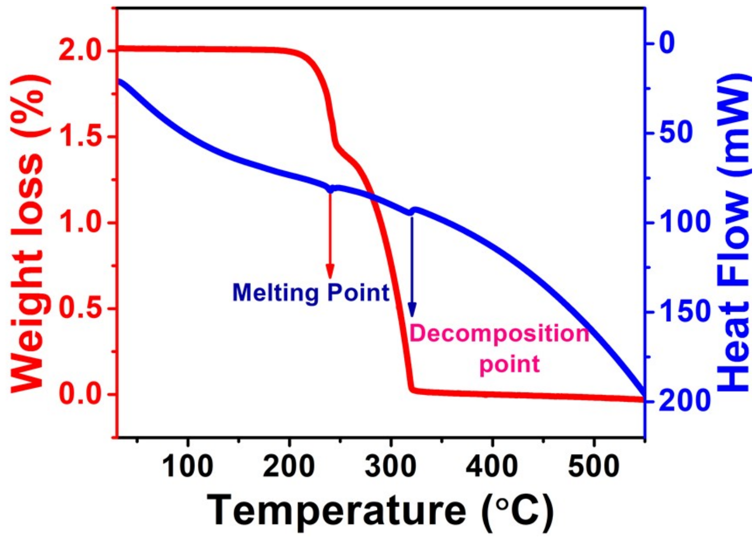

Figure S4. The thermogravimetric and differential thermal analysis profiles of **1-S**.

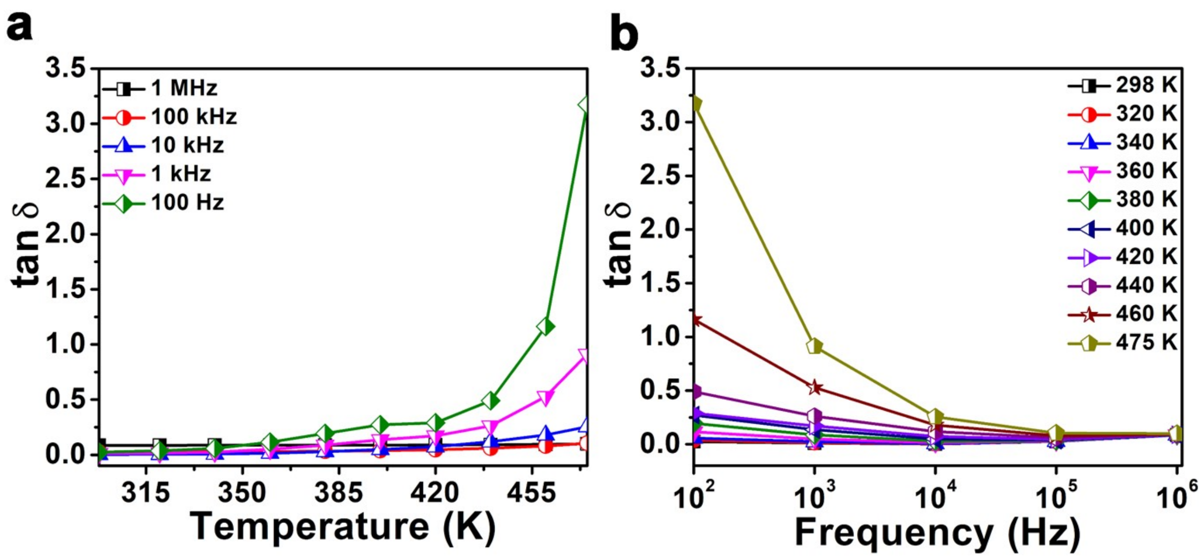

Figure S5. (a) Temperature dependant dielectric loss plot and (b) Frequency dependant dielectric loss plot of **1-S**.

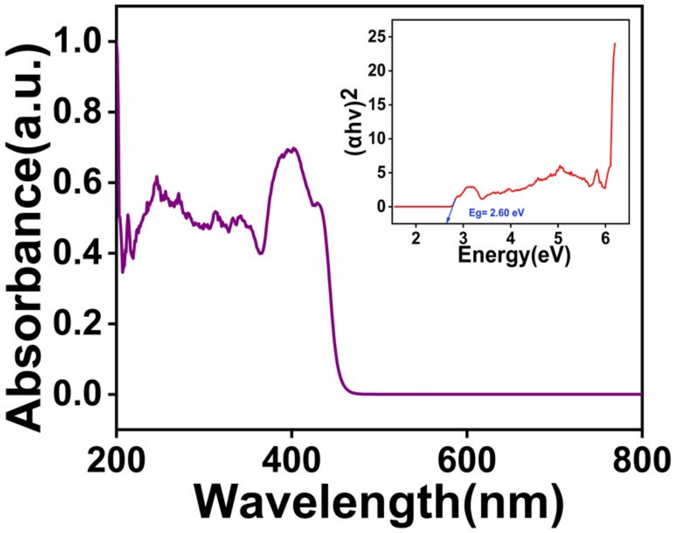

Figure S6. UV-Visible diffuse reflectance spectrum of **1-S;** its corresponding Tauc plot is displayed in the inset.

Table S3. Details about the preparation of various weight percentage (wt %) **1-S-**PLA composites.

Composite (wt%)	1-S (in mg)	1-S + PLA (in mg)
5 wt%	28.94	578.94
10 wt%	61.11	611.11
15 wt%	97.05	647.05
20 wt%	137.50	687.50

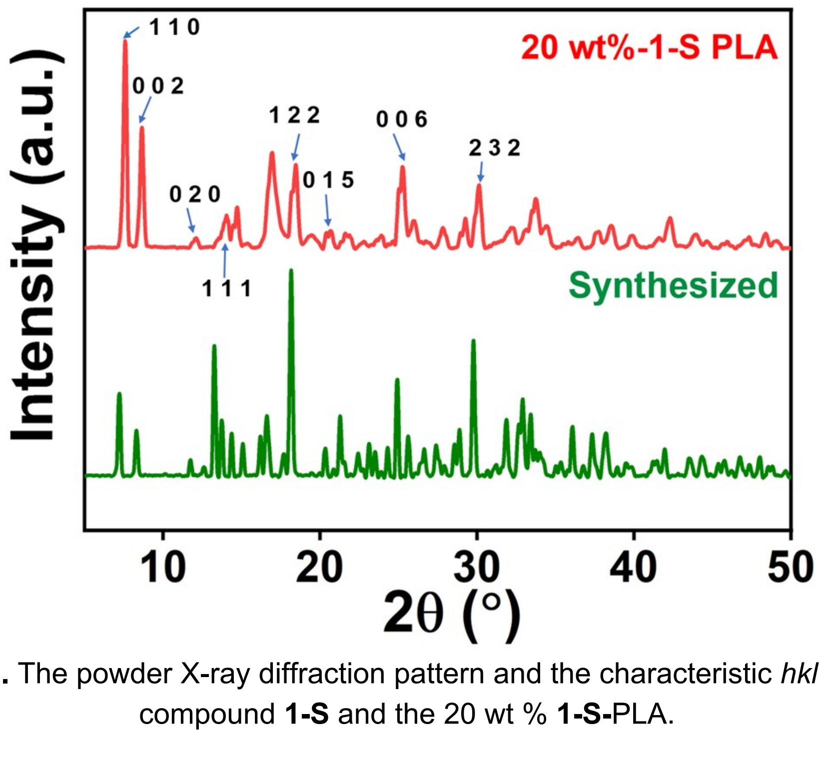

Figure S7. The powder X-ray diffraction pattern and the characteristic *hkl* peaks for compound **1-S** and the 20 wt % **1-S-**PLA.

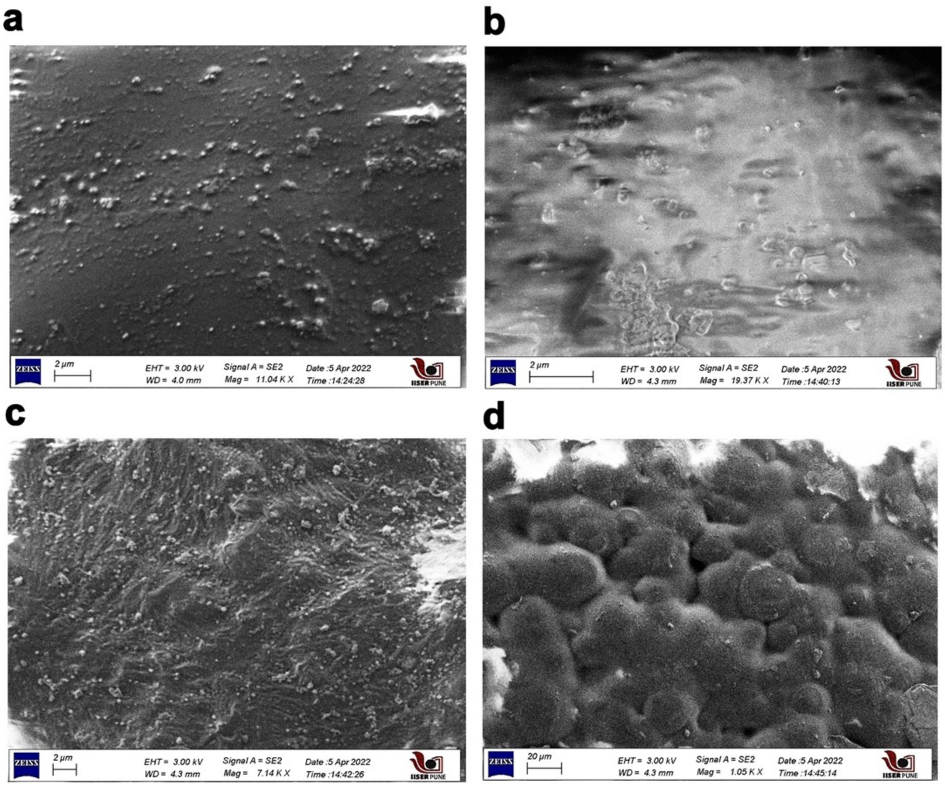

Figure S8. The FE-SEM images of **1-S-**PLA composites. The figures a, b, c, and d correspond to 5, 10, 15, and 20 wt % **1-S-**PLA composites respectively.

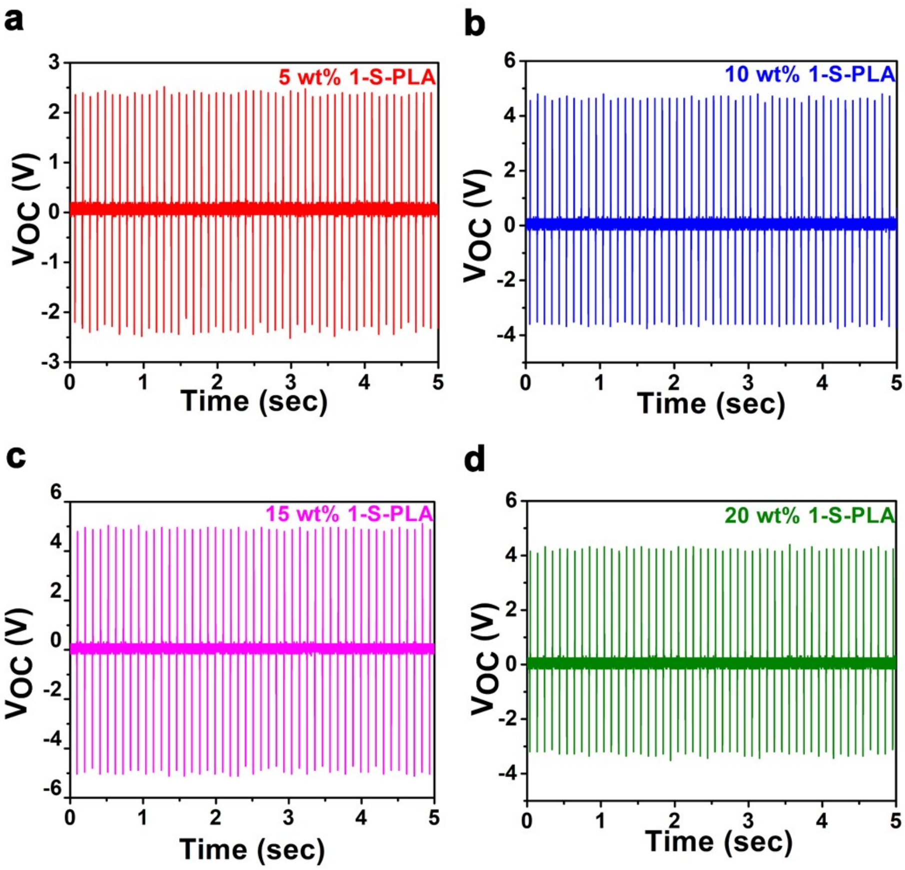

Figure S9. Output voltage profiles of all the **1-S-**PLA composite films.

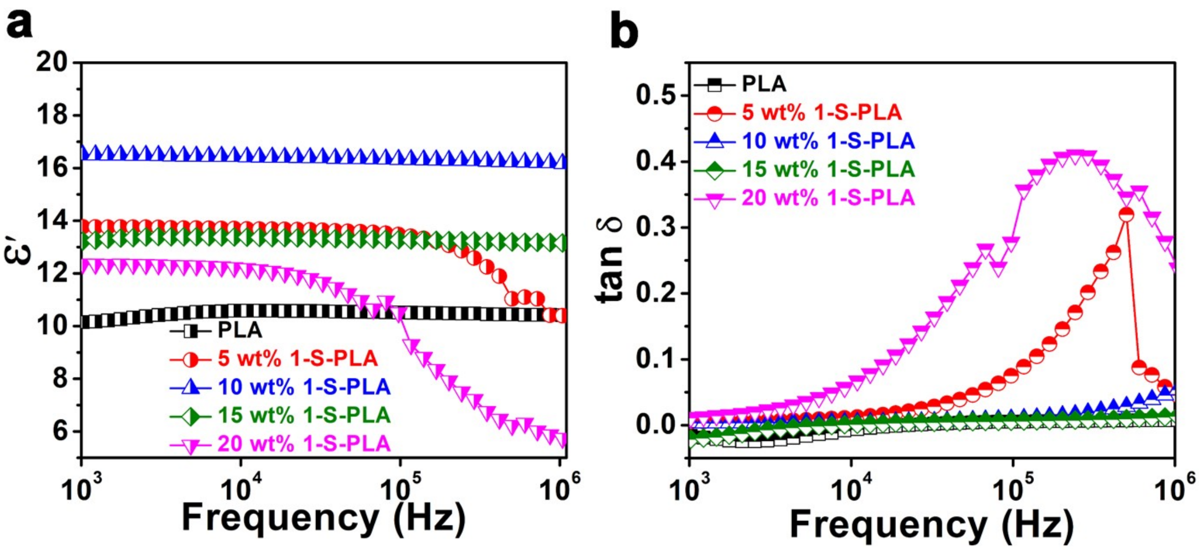

Figure S10. Frequency dependent dielectric permittivity and (b) Frequency dependent dielectric loss plot of neat PLA and all **1-S-**PLA films.

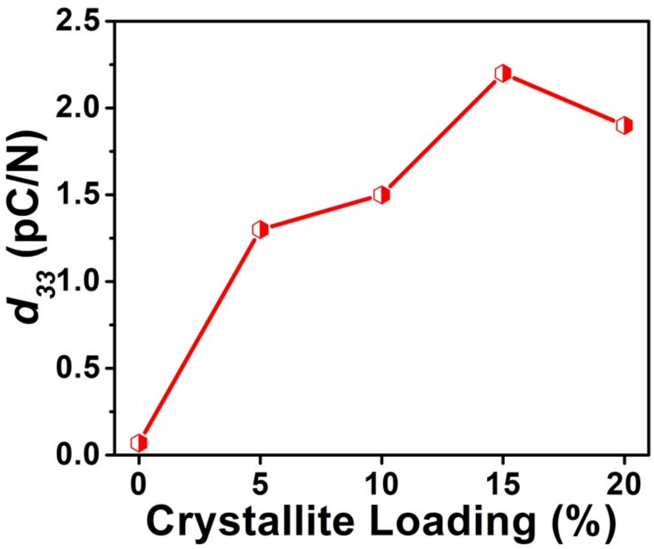

Figure S11. The comparative d_{33} values for all **1-S-**PLA composite films and neat PLA film. The solid lines the connecting the points are a guide the eye.

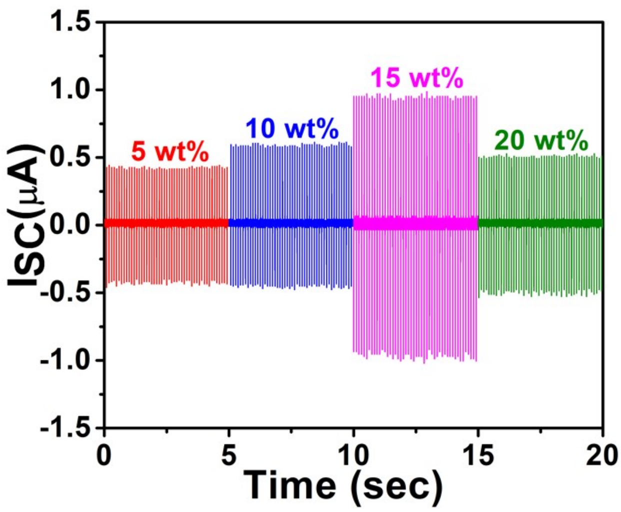

Figure S12. Output current profile of **1-S-**PLA composite films.

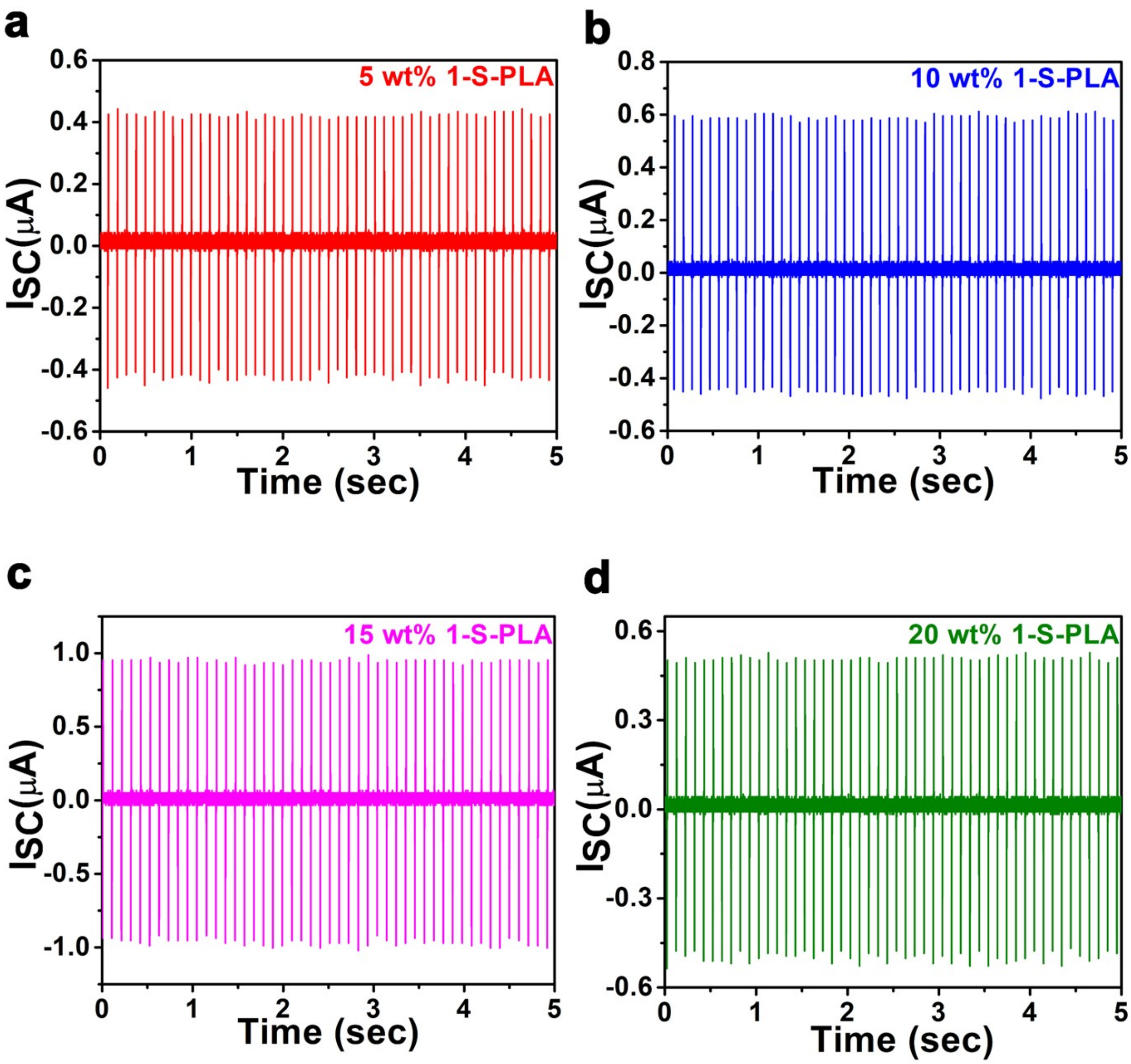

Figure S13. The calculated output currents of all the **1-S-**PLA composite films.

Table S4. Summary of maximum piezoelectric energy harvesting outputs of 15 wt% **1-S**-PLA composite devices.

Parameters	Energy Harvesting Outputs
Area of the Device	3.6 cm^2
Maximum V_{PP}	10.4 V
Maximum I_{PP}	2.2 μA
Maximum CD	0.5 $\mu A/cm^2$
Maximum PD	5.26 $\mu W/cm^2$
Energy Stored in 100 μF Capacitor	58.25 μJ
Charge Stored in 100 μF Capacitor	116.5 μC

Table S5. Comparison of output device performances of known energy harvesters based on polymer composites of organic-inorganic hybrid materials.

Hybrid Composite Devices	Output Voltages	Current/Current density	Power/Power density	Active area	References
$MAPbI_3$-PVDF	9.43	0.76 µA cm^{-2}	-	1 x 1 cm^2	1
$MAPbBr_3$-PVDF	5	60 nA	0.28 µW cm^{-2}	2.4 x 1.5 cm^2	2
$MAPbI_3$-PDMS	1.0	50 nA cm^{-2}	-	1 x 1 cm^2	3
$FAPbBr_3$–PDMS	4	-	-	1 x 1 cm^2	4
$CsPbBr_3$/PVDF	10.3	1.29 µA cm^{-2}	3.31 µW	1 x 1 cm^2	5
PVDF–PLLA–SnO_2 NF–$MAPbI_3$	4.82	29.7 nA	-	0.25 x 0.25 cm^2	6
SnO_2 NF–$MAPbI_3$	1.02	10.32 nA	-	0.25 x 0.25 cm^2	6
$[BnNMe_3]_2CdBr_4$/PDMS	52.9	0.23 µA cm^{-2}	13.8 µW cm^{-2}	3 x 3 cm^2	7
$[BnNMe_2{}^nPr]_2CdBr_4$/PDMS	63.8	0.59 µA cm^{-2}	37.1 µW cm^{-2}	3 x 3 cm^2	7
$(TMFM)FeBr_4$	2.2	-	-	-	8
$[Ph_3MeP]_4[Ni(NCS)_6]$/TPU	19.29	3.59 µA cm^{-2}	2.51 mW cm^{-3} (50.26 µW cm^{-2})	1.3 x 3 cm^2	9
$[Ph_3MeP]_2[CuCl_4]$/TPU	25	1.1 µA cm^{-2}	14.1 µW cm^{-2}	1.2 x 3 cm^2	10
15 wt% 1-S-PLA	**10.4**	**0.5 µA cm^{-2}**	**5.26 µW cm^{-2}**	**1.2 x 3 cm^2**	**This work**

Note: $MAPbI_3$ = methylammonium lead iodide; PVDF = polyvinylidene difluoride; PDMS = polydimethysiloxane; $FAPbBr_3$ = formamidinium lead bromide; PLLA = poly(L-lactic acid); SnO_2 = tin oxide; NF = nanofiber; $[BnNMe_3]_2CdBr_4$ = N,N,N-trimethyl-1-phenylmethanaminium cadmium(II) bromide; $[BnNMe_2{}^nPr]_2CdBr_4$ = N-benzyl-N,N-dimethylpropan-1-aminium cadmium(II) bromide; $(TMFM)FeBr_4$ = trimethylfluoromethylammonium iron(III)bromide, TPU = thermoplastic polyurethane, PLA = polylactic acid .

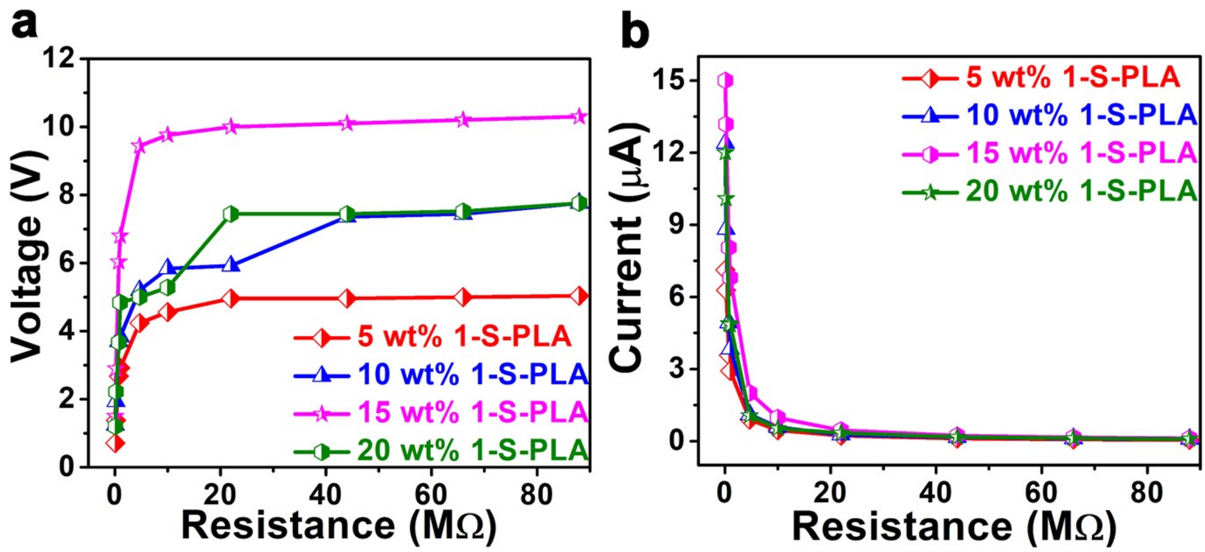

Figure S14. The comparative output (a) voltage and (b) current data for all the **1-S-**PLA composite devices under various load resistances.

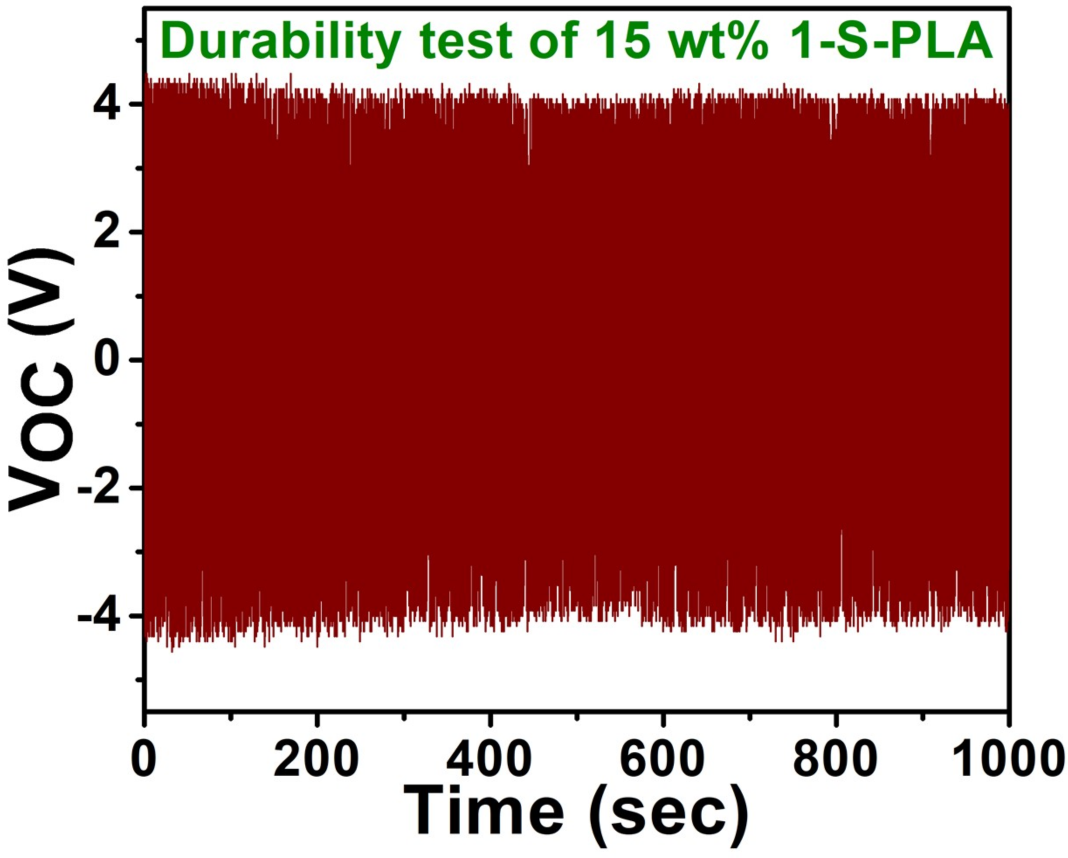

Figure S15. Fatigue test for the 15 wt% **1-S-**PLA composite device up to 10000 cycles.

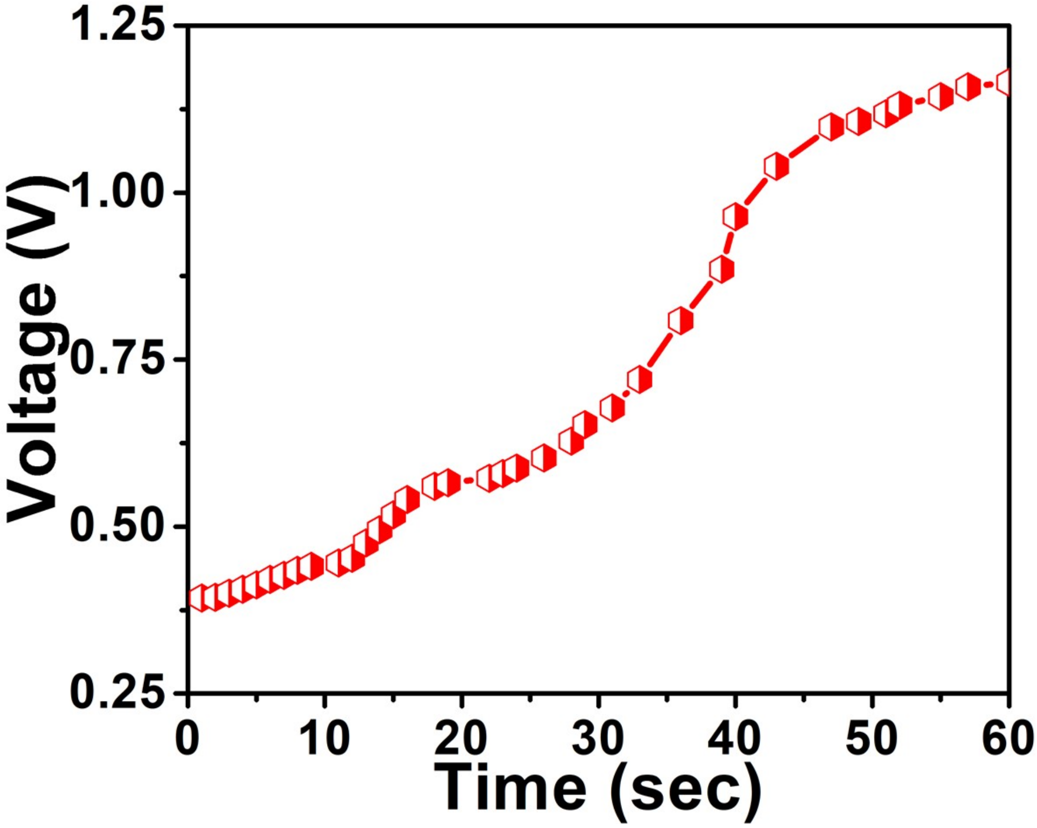

Figure S16. Stored voltages in a 100 μF capacitor by employing the 15 wt % **1-S-**PLA composite device at different time intervals.

References

1. V. Jella, S. Ippili, J.-H. Eom, J. Choi and S.-G. Yoon, *Nano Energy*, 2018, **53**, 46-56.
2. A. Sultana, M. M. Alam, P. Sadhukhan, U. K. Ghorai, S. Das, T. R. Middya and D. Mandal, *Nano Energy*, 2018, **49**, 380-392.
3. Y.-J. Kim, T.-V. Dang, H.-J. Choi, B.-J. Park, J.-H. Eom, H.-A. Song, D. Seol, Y. Kim, S.-H. Shin, J. Nah and S.-G. Yoon, *Journal of Materials Chemistry A*, 2016, **4**, 756-763.
4. R. Ding, H. Liu, X. Zhang, J. Xiao, R. Kishor, H. Sun, B. Zhu, G. Chen, F. Gao, X. Feng, J. Chen, X. Chen, X. Sun and Y. Zheng, *Advanced Functional Materials*, 2016, **26**, 7708-7716.
5. Y. Li, M.-h. Xu, Y.-s. Xia, J.-m. Wu, X.-k. Sun, S. Wang, G.-H. Hu and C.-x. Xiong, *Chemical Engineering Journal*, 2020, **388**, 124205.
6. R. Tusiime, F. Zabihi, M. Tebyetekerwa, Y. M. Yousry, Y. Wu, M. Eslamian, S. Yang, S. Ramakrishna, M. Yu and H. Zhang, *Journal of Materials Chemistry C*, 2020, **8**, 2643-2658.
7. S. Deswal, S. K. Singh, P. Rambabu, P. Kulkarni, G. Vaitheeswaran, B. Praveenkumar, S. Ogale and R. Boomishankar, *Chemistry of Materials*, 2019, **31**, 4545-4552.
8. Y. Zhang, X.-J. Song, Z.-X. Zhang, D.-W. Fu and R.-G. Xiong, *Matter*, 2020, **2**, 697-710.
9. T. Vijayakanth, F. Ram, B. Praveenkumar, K. Shanmuganathan and R. Boomishankar, *Angewandte Chemie International Edition*, 2020, **59**, 10368-10373.
10. S. Sahoo, T. Vijayakanth, P. Kothavade, P. Dixit, J. K. Zaręba, K. Shanmuganathan and R. Boomishankar, *ACS Materials Au*, 2022, **2**, 124-131.

.